Cold Sintered C0G Multilayer Ceramic Capacitors

Dawei Wang[1]*, Di Zhou[2], Kaixin Song[1,3], Antonio Feteira[4], Clive A. Randall[5], Ian M Reaney[1]*

Dr. D. Wang 1, Prof. D. Zhou 2, Prof. K. Song 1,3, Dr. A. Feteira 4, Prof. C. A. Randall 5, Prof. I. M. Reaney 1
1 Department of Materials Science and Engineering, University of Sheffield, Sheffield S1 3JD, UK
2 Electronic Materials Research Laboratory, Key Laboratory of the Ministry of Education & International Center for Dielectric Research, Xi'an Jiaotong University, Xi'an 710049, Shaanxi, China
3 College of Electronic Information and Engineering, Hangzhou Dianzi University, Hangzhou 310018, China
4 Christian Doppler Laboratory for Advanced Ferroic Oxides, Sheffield Hallam University, Sheffield S1 1WB, UK
5 Materials Research Institute, The Pennsylvania State University, University Park, PA 16802, USA
E-mail: dawei.wang@sheffield.ac.uk, i.m.reaney@sheffield.ac.uk

Novel multilayer ceramic capacitors (MLCCs) based on a $(Bi_{0.95}Li_{0.05})(V_{0.9}Mo_{0.1})O_4$-$Na_2Mo_2O_7$ (BLVMO-NMO), with $\varepsilon_r = 39$, temperature coefficient of capacitance, TCC ~ +/- 0.01% and $tan\delta = 0.01$ at 1 MHz, were successfully fabricated by a cold sintering process at 150 °C. Scanning electron microscopy of MLCCs combined with EDS mapping, X-ray diffraction and Raman spectroscopy revealed well-laminated and undistorted dielectric layers composed of BLVMO and NMO discrete phases separated by Ag internal electrodes. Prototypes showed comparable properties to C0G MLCCs (TCC = +/-30 ppm/°C from -55 to +125 °C) currently commercially fabricated at 1100 °C using $CaZrO_3$ based dielectrics with glass sintering aids and Ni internal electrodes.

Introduction

Modern wireless communication systems and electronic packaging rely on passive components such as antennas, resonators, filters and capacitors.[1,2] Invariably these components are based on functional ceramics which meet stringent technical specifications, in particular low dielectric loss or high quality factor *(Q)* and low temperature coefficient of resonant frequency (TCF) or capacitance (TCC). The ever-increasing trend towards miniaturisation of electronic systems drives the 3D integration of alternating ceramic and metallic electrode layers. Multilayer ceramic capacitors (MLCCs) are probably the best known and most successful examples of 3D integration of functional ceramics with more than two trillion manufactured every year.[3-5] 3D integration demands the sintering temperature of the ceramic layers is lower than the melting temperature of (and chemically compatible with) the metallic electrode.[6-10] These requirements have led to four typical categories of dielectrics based on their sintering temperature: i) high-temperature co-fired ceramics (HTCC, 1200-1800°C); ii) low-temperature co-fired ceramics (LTCC, 900-1000°C); iii) ultra-low temperature co-fired ceramics (ULTCC, 400-700°C), and more recently iv) cold-sintered co-fired ceramics (CSCC, 20-200°C).[6-15] The major drawback of HTCC systems is the need to use high melting temperature metallic electrodes, such as Pt, Pd, Au or related alloys. Successive developments in LTCC and ULTCC systems have permitted the use of low melting metal electrodes, such Ag, Cu, Al, which are considerably cheaper.[16-17] Nevertheless, in many of these LTCC/ULTCC systems it is not always possible to prevent the reaction between the ceramic and electrodes. These reactions are accompanied by either the formation of parasitic phases and/or modification of the electrical properties due to interdiffusion[12,18-20] which impairs the functionality of the device. Recently, CSCC has emerged as a new processing route to overcome some of the electrode compatibility issues faced by LTCC/ULTCC systems. This new technology allows densification at temperatures ≤ 200°C,[11,20-30] thereby offering a great opportunity to manufacture MLCCs co-fireable with

2

most types of electrode. In addition, CSCC also reduces the carbon footprint (CO_2 emissions) inherent in conventional high temperature sintering.[21]

Recently, the cold sintering process (CSP) has been successfully employed to fabricate microwave bulk ceramics, such as Li_2MoO_4, $Na_2Mo_2O_7$, $K_2Mo_2O_7$, NaCl, $(LiBi)_{0.5}MoO_4$, Li_2MoO_4-PTFE, $Na_{0.5}Bi_{0.5}MoO_4$-Li_2MoO_4 and Al_2SiO_5-NaCl[11,20-30] but no prototype cold-sintered MLCCs have been fabricated whose properties match those commercially available.[31-34] MLCCs are categorised according to the Electronic Industry Alliance codes which specify the operating window and their required temperature stability. X7R MLCCs are based on modified $BaTiO_3$ ($\varepsilon_r > 2000$) with TCC = +/-15% of the RT value between -55 to +125 °C. C0G MLCCs are fabricated from dielectrics such as $CaZrO_3$ (+ glass frit) with lower ε_r (30-40) but with TCC $\leq$ +/-30 ppm/°C.

In this work, $(Bi_{0.95}Li_{0.05})(V_{0.9}Mo_{0.1})O_4$ (BLVMO) and $Na_2Mo_2O_7$ (NMO) ceramics with positive and negative TCF of ~ +81 ppm/°C and -99 ppm/°C, respectively, were selected as end-members to fabricate novel temperature stable BLVMO-NMO composites.[20,35-37] Temperature stable (< 10 ppm/°C) composites with low dielectric loss ($tan\delta$ ~ 0.001) and ε_r = 40 were attained which were subsequently used to fabricate MLCCs at 150 °C. The MLCCs corresponded to C0G, the current commercial incarnation of which, is conventionally sintered at ~1100 °C with sales in excess of 100 billion parts per year.

Experimental Section

BLVMO and NMO powders were synthesized separately by the solid-state reaction method. Raw materials, including Bi_2O_3 (99.9%, Acros Organics), MoO_3 (99+%, Acros Organics), VO_3 (99+%, Acros Organics), Li_2CO_3 (99.9%, Sigma-Aldrich) and Na_2CO_3 (99.9%, Fisher Scientific) were batched stoichiometrically according to the nominal compositions and

planetary ball-milled in isopropanol for 4 h. The dried mixed powders were calcined at

600 °C for BLVMO and 500 °C for NMO, respectively, to synthesize the compounds.

Subsequently, BLVMO and NMO powders were weighted in 4:1 ratio and ball-milled in

isopropanol for 24 h. After drying, the BLVMO-NMO formulation was employed to fabricate

MLCCs following the previous work of Guo et al.[11] Ceramic tapes were made by tape casting

(Compact Tape caster, MTI) and electroded using a screen-printer (247 screen printer, DEK)

and Ag paste (LTC3602, Heraeus Electronics). Electroded tapes were stacked and laminated

at 80 °C for 20 mins (Atlas Heated Platens, Specac) under an uniaxial pressure of 10 MPa.

After binder burnout at 180 °C for 3 hrs, the laminated BLVMO-NMO tapes were wetted by

exposing to water vapor in a sealed beaker at 80 °C. Finally, to fabricate the MLCCs, the

moistened tapes were put into a die and cold sintered at 150 °C for 30 minutes under a

uniaxial pressure of 100 MPa, schematically illustrated in Figure 1. After drying at 120 °C for

24 h to remove any residual moisture, a Ag terminal electrode (LTC3602, Heraeus

Electronics) was applied onto MLCCs before performing electrical measurements. For

comparison, cold-sintered BLVMO, NMO and BLVMO-NMO bulk ceramics were prepared

under the same conditions as the MLCCs. In addition, BLVMO and NMO bulk ceramics were

conventionally sintered at 690 and 610°C, respectively.

Bulk densities of ceramic pellets were calculated by the geometric method. Crystal structure,

phase assemblage, microstructures and Raman spectra of MLCCs and ceramic pellets were

characterised by X-ray powder diffraction (XRD, D2 Phaser, Bruker) using Cu$K\alpha$ radiation,

scanning electron microscopy (SEM, Inspect F, FEI) and Raman spectroscopy (inVia Raman

microscope, Renishaw) using a green laser with 514.5 nm at room temperature, respectively.

Microwave properties of ceramic pellets were measured using the $TE_{01\delta}$ dielectric resonator

method with a vector network analyzer (R3767CH, Advantest Corporation, Tokyo, Japan). A

Peltier device was used to heat the cavity to measure the resonant frequency (f) from 25 °C to

85 °C. The TCF was calculated using the following formula:

$$TCF = \frac{f_T - f_{T_0}}{f_{T_0} \times (T - T_0)} \times 10^6 \qquad (1)$$

where the f_T and f_{T_0} were the TE$_{01\delta}$ resonant frequencies at temperature T and T$_0$,

respectively. The temperature dependence of dielectric properties from room temperature to

150 °C was carried out using an Agilent 4184A multi-frequency precision LCR meter. The

temperature coefficient of capacitance (TCC) was calculated using Equation (2),

$$TCC = \Delta\varepsilon_r / (\varepsilon_{25}\Delta T), \qquad (2)$$

where ε_{25} is ε_r at 25 °C, $\Delta\varepsilon_r$ and ΔT is the change in relative permittivity (ε_r) and temperature,

relative to ε_{25} and 25 °C.

Results and discussion

Relative densities (ρ_r) and microwave dielectric properties of BLVMO, NMO and BLVMO-

NMO ceramics cold-sintered at 150 °C are compared in Table I with those of BLVMO, NMO

ceramics conventionally sintered at 690 °C and 610 °C, respectively. Cold-sintered NMO

ceramics exhibit a slightly larger ε_r than their conventionally sintered counterparts,

commensurate with the enhancement of ρ_r from 87 to 95%. Conversely, cold-sintered

BLVMO ceramics exhibit remarkably lower ε_r than their conventionally sintered counterparts

which were only 73% relative density. The lower Qf of cold-sintered BLVMO ceramics can

be ascribed to the low density of this end member but all cold-sintered composites with NMO

attained ρ_r > 94%. Most notably, composites with 20 wt% NMO and 80 wt% BLVMO exhibited ε_r ~ 40, Qf ~ 4000 and TCF of +4 ppm/°C.

Room-temperature XRD patterns of cold-sintered BLVMO, NMO and BLVMO-NMO samples in the 2θ range of 10°~50° are shown in Figure 2(a). BLVMO has a tetragonal scheelite structure,[35-37] with no evidence of splitting of main diffraction peaks. NMO has an orthorhombic structure with symmetry described by the space group Cmca (PDF 01-073-1797, a = 7.164 Å, b = 11.837 Å, c = 14.713 Å, Z = 8).[20] All reflections in the XRD data for BLVMO-NMO ceramic composites can be ascribed to BLVMO and NMO and there is no apparent shift in peak position, indicating no interaction between these two end members.

Room-temperature Raman spectra of cold-sintered BLVMO, NMO and BLVMO-NMO ceramics are shown in Figure 2(b). Based on group theory and irreducible representations, there are 15 and 129 different vibrational modes in BLVMO and NMO,[35-38] respectively, given as follows:

$\Gamma_{BLVMO} = 3A_g + 2A_u + 6B_g + 4B_u$

$\Gamma_{NMO} = 18A_g + 13A_u + 15B_{1g} + 19B_{1u} + 14B_{2g} + 18B_{2u} + 19B_{3g} + 13B_{3u}$.

In BLVMO, nine $3A_g + 6B_g$ modes are Raman active and six $2A_u + 4B_u$ modes are IR active.[35-37] In NMO, translations of Na and Mo atoms contribute to $3A_g + 2A_u + 3B_{1g} + 4B_{1u} + 3B_{2g} + 4B_{2u} + 3B_{3g} + 2B_{3u}$ and $3A_g + 2A_u + 3B_{1g} + 4B_{1u} + 2B_{2g} + 3B_{2u} + 4B_{3g} + 3B_{3u}$ modes, respectively. Three $B_{1u} + B_{2u} + B_{3u}$ modes are acoustic active and the remaining $12A_g + 9A_u + 9B_{1g} + 12B_{1u} + 9B_{2g} + 12B_{2u} + 19B_{3g} + 9B_{3u}$ modes correspond to stretching and bending modes of MoO_4 and MoO_6 octahedra.[38] The Raman spectrum of BLVMO-NMO composites consists of a superposition of the spectral features exhibited by each individual phase, further confirming the coexistence of BLVMO and NMO in composite ceramics.

Back-scattered electron (BSE) images of fracture surface of cold-sintered BLVMO-NMO

MLCCs are shown in Figure 2(c,d). Image contrast shows the microstructures to encompass two chemically distinct and discrete phases with EDS attributing the dark and light contrast regions to NMO and BLVMO, respectively, in agreement with the XRD and Raman results (Figure 2 a,b). The grain size of NMO (5-10 μm) is much larger than that of BLVMO (1-2 μm), consistent with previous reports.[20,35-37] Figure 2(c) shows a ~ 10 μm silver electrode layer, which has sharp interface with the ceramic grains, supporting good chemical compatibility between grains of the composite and the Ag-electrode.

An SEM image of a cross-section of 9-layered BLVMO-NMO MLCC is given in Figure 3(a). It shows a dense, well-laminated and unwarped MLCC consisting of ceramic layers of ~ 200 μm thick separated by continuous Ag-electrodes. EDS mapping shows a random distribution of chemical elements, Figure 3 (b-h), consistent with a random distribution of the BLVMO and NMO grains. Furthermore, at such a low temperature no reaction at the ceramic/metal interface is detected. A key processing advantage of CSP, besides the low processing temperature, is the absence of lateral shrinkage which allows fabrication of novel and dense MLCCs without delamination and warping, as shown in Figure 3(a).

The temperature dependence of dielectric properties and TCC for MLCCs measured in the 1 kHz-1 MHz is shown in Figure 4. Both relative permittivity (ε_r) and dielectric loss ($tan\delta$) are stable up to 150 °C (except 1 kHz) but decrease with increasing frequency. The room-temperature, ε_r and $tan\delta$ at 1 MHz are 39 and 0.01, respectively, consistent with those measured at MW frequencies, Table I. For lower frequencies ($\leq$ 10 KHz), ε_r and $tan\delta$ rise due to space charge dependent conductivity. No attempt has been made to measure the properties below RT but projections of the curves suggest ε_r and $tan\delta$ will remain constant. TCC increases with decreasing frequency but for 1MHz (the lowest likely operating frequency) the values lie well within C0G limits of < 30 ppm/ºC or 0.01% of the RT value to 150 °C in

agreement with the near-zero TCF of the ceramics in Table I.

Conclusions

In this work, BLVMO-NMO MLCCs were successfully fabricated by a cold sintering at

150 °C. XRD, Raman, electron microscopy and EDS mapping showed that the composites

were chemical compatible with the Ag internal electrodes. MLCCs were temperature stable

within C0G at 1 MHz from room-temperature to 150°C. This is the first demonstration

therefore, of a cold sintered prototype RF component whose properties match those of

commercial MLCCs fabricated using conventional sintering.

Conflict of Interest: The authors declare no conflict of interest.

Received: ((will be filled in by the editorial staff))
Revised: ((will be filled in by the editorial staff))
Published online: ((will be filled in by the editorial staff))

References

[1]   I. M. Reaney, D. Iddles, *J. Am. Ceram. Soc.* **2006**, *89*, 2063.

[2]   D. Zhou, L. Pang, **D. Wang**, I. M. Reaney, *J. Mater. Chem. C* **2018**, *6*, 9290.

[3]   J. Ho, T. R. Jow, and S. Boggs, *IEEE Electr. Insul. Mag.* **2010**, *26*, 20.

[4]   P. Y. Foeller, J. S. Dean, I. M. Reaney, and D. C. Sinclair, *Appl. Phys. Lett.* **2016**, *109*,

082904.

[5]   D. Zhou, C. A. Randall, A. Baker, H. Wang, L. Pang, X. Yao, *J. Am. Ceram. Soc.* **2010**,

93, 1443.

[6]   M. T. Sebastian, H. Jantunen, *Int. Mater. Rev.* **2008**, *53*, 57.

[7]   H. Yu, J. Liu, W. Zhang, S. Zhang, *J. Mater. Sci.: Mater. Electron.* **2015**, *26*, 9414.

[8]   D. Zhou, L. Pang, **D. Wang**, Z. Q, I. M. Reaney, *ACS Sus. Chem. Eng.* **2018**, *6*, 11138.

[9]   D. Zhou, L. Pang, **D. Wang**, C. Li, B. Jin, I.M. Reaney, *J. Mater. Chem. C*, **2017**, *5*, 10094.

[10]   D. Zhou, J. Li, L. Pang, **D. Wang**, I. M. Reaney, *J. Mater. Chem. C*, **2017**, *5*, 6086.

[11]   J. Guo, A. L. Baker, H. Guo, M. T. Lanagan, C. A. Randall, *J. Am. Ceram. Soc.* **2017**, *100*, 669.

[12]   D. Zhou, C. A. Randall, H. Wang, L. X. Pang, X. Yao, *J. Am. Ceram. Soc.* **2010**, *93*, 1096.

[13]   M. T. Sebastian, H. Wang, H. Jantunen, Curr. Opin. *Solid State Mater. Sci.* **2016**, *20*, 151.

[14]   M. Udovic, M. Valant, D. Suvorov, *J. Am. Ceram. Soc.* **2004**, *8*, 591.

[15]   Y. Imanaka, Multilayered Low Temperature Cofired Ceramics (LTCC) Technology. New York: Springer; 2005.

[16]   H. Yu, J. Liu, W. Zhang, S. Zhang, *J. Mater. Sci.: Mater. Electron.* **2015**, *26*, 9414.

[17]   M. J. Pan, C. A. Randall, *IEEE Electr. Insul. Mag.* **2010**, *26*, 44.

[18]   D. Zhou, H. Wang, L. X. Pang, C. A. Randall, X. Yao, *J. Am. Ceram. Soc.* **2009**, *92*, 2242.

[19]   D. Zhou, W. B. Li, L. X. Pang, J. Guo, Z. M. Qi, T. Shao, Z. X. Yue, X. Yao, *J. Am. Ceram. Soc.* **2014**, *97*, 3597.

[20]   G. Q. Zhang, H. Wang, J. Guo, L. He, D. D. Wei, Q. B. Yuan, *J. Am. Ceram. Soc.* **2015**, *98*, 528.

[21]   T. Ibn-Mohammed, C. A. Randall, K. B. Mustapha, J. Guo, J. Walker, S. Berbano, S. C. L. Koh, D. C. Sinclair, I. M. Reaney, Decarbonising ceramic manufacturing: a techno-

economic analysis of energy efficient sintering technologies in the functional materials

sector, submitted.

[22]   D. Wang, D. Zhou, S. Zhang, Y. Vardaxoglou, W.G. Whittow, D. Cadman, I.M. Reaney, *ACS Sus. Chem. Eng.* **2018**, *6*, 2438.

[23]   H. Kähäri, M. Teirikangas, J. Juuti, H. Jantunen, *J. Am. Ceram. Soc.* **2014**, *97*, 3378.

[24]   H. Kähäri, M. Teirikangas, J. Juuti, H. Jantunen, *Ceram. Inter.* **2016**, *42*, 11442.

[25]   I. J. Induja, M. T. Sebastian, *J. Euro. Ceram. Soc.* **2017**, *37*, 2143.

[26]   M. Väätäjä, H, Kähäri, J. Juuti, H. Jantunen, *J. Am. Ceram. Soc.* **2017**, *100*, 3626.

[27]   M. Väätäjä, H, Kähäri, K. Ohenoja, M. Sobocinski, J. Juuti, H. Jantunen, *Sci. Rep.* **2018**, *8*, 15955.

[28]   J. Guo, H. Guo, A. L. Baker, M. T. Lanagan, E. R. Kupp, G. L. Messing, C. A. Randall, *Angew. Chem. Int. Ed.* **2016**, *55*, 11457.

[29]   J. Guo, S. S. Berbano, H. Guo, A. L. Baker, M. T. Lanagan, C. A. Randall, *Adv. Funct. Mater.* **2016**, *26*, 7115.

[30]   W. Hong, L. Li, M. Cao, X. M. Chen, *J. Am. Ceram. Soc.* **2018**, *101*, 4038.

[31]   D. Zhou, D. Guo, W. B. Li, L. X. Pang, X. Yao, D. W. Wang, I. M. Reaney, *J. Mater. Chem. C* **2016**, *4*, 5357.

[32]   D. Zhou, J. Li, L. X. Pang, G. H. Chen, Z. M. Qi, D. W. Wang, I. M. Reaney, *ACS Omega* **2016**, *1*, 963.

[33]   L. Pang, D. Zhou, D. Wang, J. Zhao, W. Liu, Z. Yue, I. M. Reaney, *J. Am. Ceram. Soc.* **2018**, *101*, 1806.

[34]   D. Zhou, L. Pang, D. Wang, H. Guo, F. Yang, Z. Qi, C. Li, B. Jin, I. M. Reaney, *J. Eur. Ceram. Soc.* **2018**, *38*, 1556.

[35]   D. Zhou, W. G. Qu, C. A. Randall, L. X. Pang, H. Wang, X. G. Wu, J. Guo, G. Q. Zhang, L. Shui, Q. P. Wang, H. C. Liu, X. Yao, *Acta Mater.* **2011**, *59*, 1502.

[36] D. Zhou, L. X. Pang, W. G. Qu, C. A. Randall, J. Guo, Z. M. Qi, T. Shao, X. Yao, *RSC Adv.* **2013**, *3*, 5009.

[37] D. Zhou, C. A. Randall, H. Wang, L. X. Pang, X. Yao, *J. Am. Ceram. Soc.* **2010**, *93*, 2147.

[38] G. D. Saraiva, W. Paraguassu, M. Maczka, P. T. C. Freire, F. F. de Sousad, J. Mendes Filho, *J. Raman Spectrosc.* 2011, *42*, 1114.
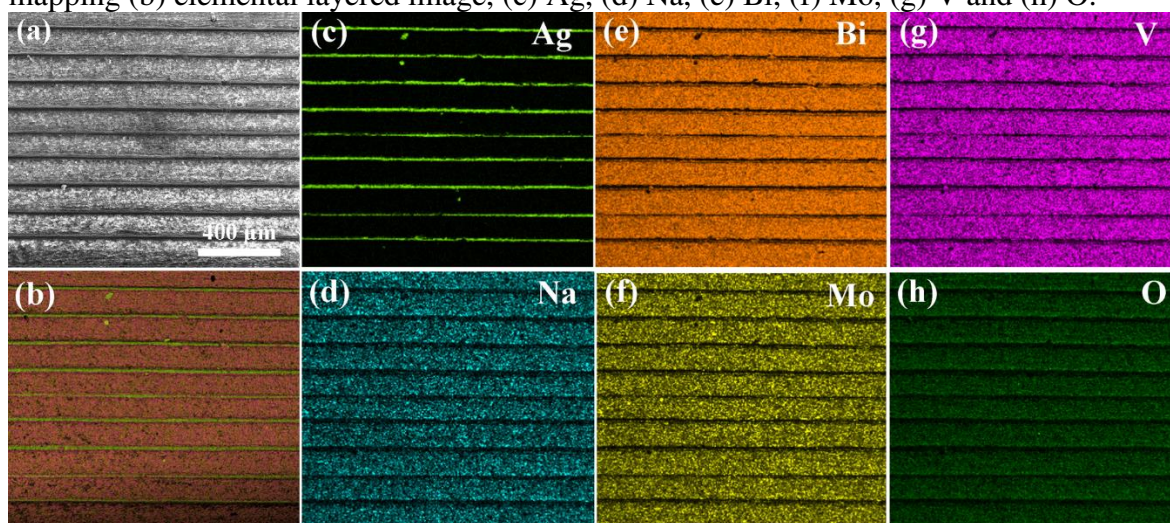
Figure 1. The schematic illustration of cold sintering process for BLVMO-NMO MLCCs.
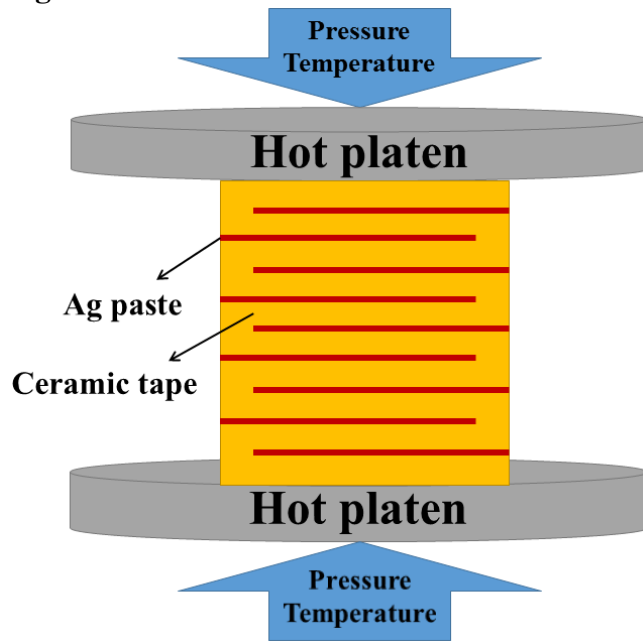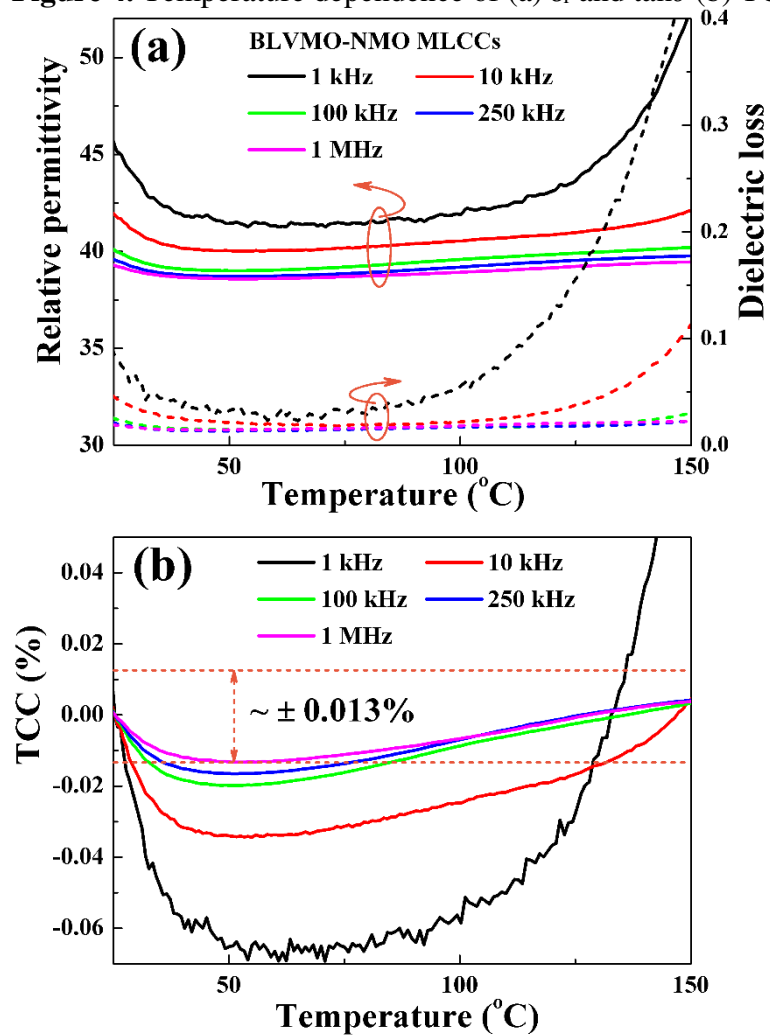
Figure 2. (a) XRD patterns, (b) Raman spectra of BLVMO, NMO and BLVMO-NMO ceramics; (c,d) BSE images for the cross-section of BLVMO-NMO MLCCs.
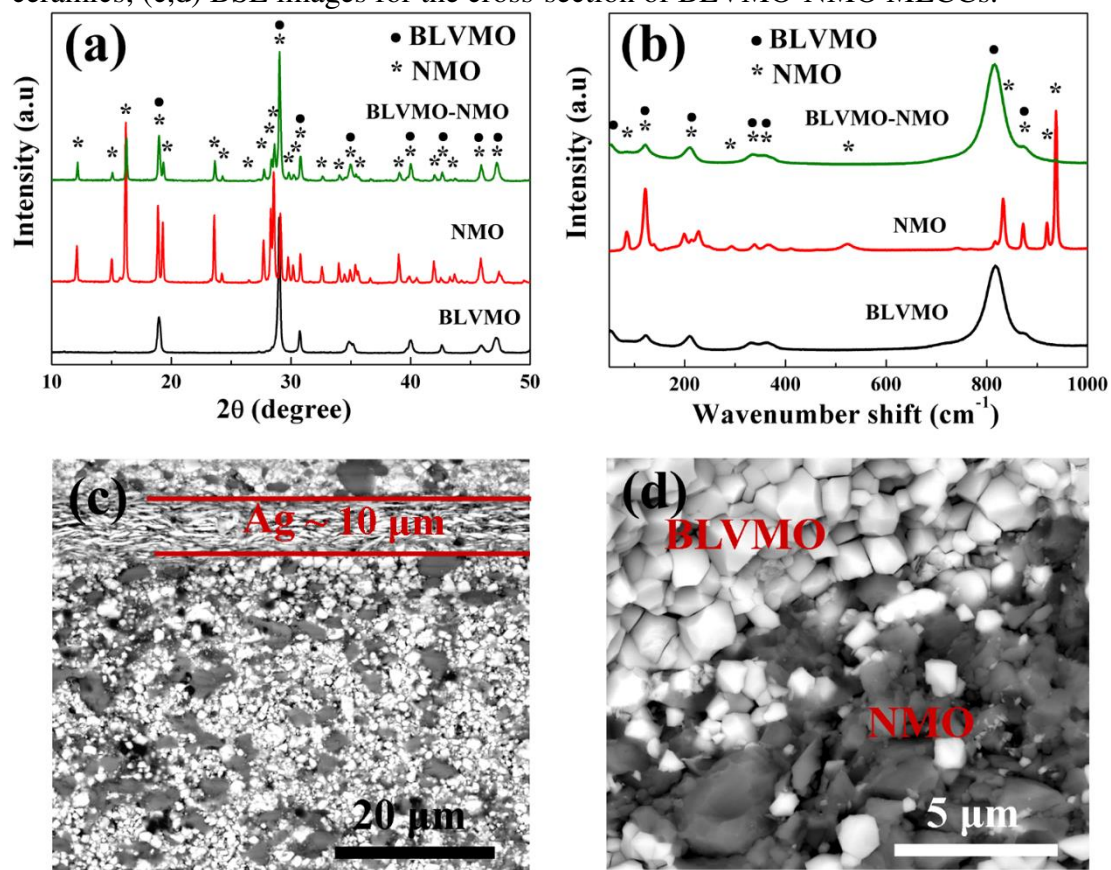
Figure 3. (a) SEM image for the cross-section of BLVMO-NMO MLCCs; and EDS elemental mapping (b) elemental layered image, (c) Ag, (d) Na, (e) Bi, (f) Mo, (g) V and (h) O.

Figure 4. Temperature dependence of (a) ε_r and tanδ (b) TCC for BLVMO-NMO MLCCs.

Table I. Sintering temperatures, relative densities, and microwave dielectric properties of BLVMO, NMO and BLVMO-NMO ceramics.

Composition	ST (°C)	ρ_r (%)	ε_r	$tan\delta$	$Q \times f$ (GHz)	TCF (ppm/°C)
BLVMO	150	73	30	0.003	1300	+61
NMO	150	95	12.7	0.0005	12000	-99
BLVMO-NMO	150	96	40	0.0012	4000	+4
BLVMO	690	96	76	0.0006	7000	+81
NMO	610	87	11.6	0.0005	19000	-78